ELSEVIER

Composites Science and Technology 59 (1999) 1097–1107

COMPOSITES SCIENCE AND TECHNOLOGY

Determination of the dynamic response of brittle composites by the use of the split Hopkinson pressure bar

Zhouhua Li, John Lambros*

Department of Mechanical Engineering, University of Delaware, Newark, DE 19716, USA

Received 3 November 1997; received in revised form 1 June 1998; accepted 14 September 1998

Abstract

In this work a split Hopkinson pressure bar (SHPB) setup was used to test brittle, polymeric-matrix composite materials. To provide a consistent and accurate way of performing data analysis, a scheme including dispersion correction, selection of starting points, stress homogeneity and limiting strain rate has been developed. Special emphasis is placed on determining stress homogeneity numerically and experimentally, which is used as a basis for the data analysis procedure. The number of frequencies needed for adequate dispersion correction in the SHPB was found to be a substantial function of the Nyquist frequency of the data acquisition system. Experimental results for a unidirectional graphite/epoxy composite material from quasi-static and SHPB tests are provided.

Keywords: A. Polymer-matrix composites; B. Impact behavior; B. Mechanical properties; B. Strength; Dispersion

1. Introduction

The split Hopkinson pressure bar (SHPB) technique has become one of the most popular experimental techniques for the study of dynamic behavior of materials. The version of the SHPB used in the study, composed of two separate bars with a specimen sandwiched in between, was introduced by Kolsky [1]. This was based on Hopkinson's [2] original one-bar design. The original SHPB was designed for compression testing, and versions of SHPB for tension [3] and torsion [4] have subsequently been developed. Additional modifications such as the momentum trapping bar used by Nemat-Nasser et al. [5], which permits only single pulse loading on a sample, have extended the capabilities of the SHPB. Traditionally, the SHPB has been used to investigate the dynamic behavior of metals. However, in recent years there has been an interest in determining dynamic elastic and failure properties for materials such as ceramics, composites, rocks and concrete. During this process, some of the limitations of the SHPB have surfaced necessitating the reevaluation of the SHPB fundamental assumptions.

A schematic illustration of the SHPB used in this work (described in detail in Section 3) is shown in Fig. 1. A traditional analysis of the SHPB provides stress, strain rate and strain in the specimen as follows:

$$\sigma(t) = \frac{AE\varepsilon_t(t)}{A_s}, \tag{1}$$

$$\dot{\varepsilon} = -\frac{2c\varepsilon_r(t)}{L_s}, \tag{2}$$

$$\varepsilon(t) = \int_0^t \dot{\varepsilon}(\tau)\,\mathrm{d}\tau, \tag{3}$$

where A, E, and $c(=\sqrt{E/\rho}$, ρ is the mass density of the bar) are cross-sectional area, Young's modulus and wave speed of the bar, respectively. L_s and A_s are length and cross-sectional area of the specimen. $\varepsilon_r(t)$ and $\varepsilon_t(t)$ are axial strains of the reflected pulse and transmitted pulse, respectively, measured in the incident and transmitted bars as functions of time t.

The derivation of Eqs. (1)–(3) is based on the following assumptions:

1. the wave propagation in the bars is well approximated by one-dimensional elastic wave propagation theory (i.e. wave dispersion is negligible);
2. the stress and strain fields in the specimen are homogeneous;
3. the radial inertia effect of the specimen and friction effect are negligible;

* Corresponding author.

0266-3538/99/$ - see front matter
PII: S0266-3538(98)00152-3

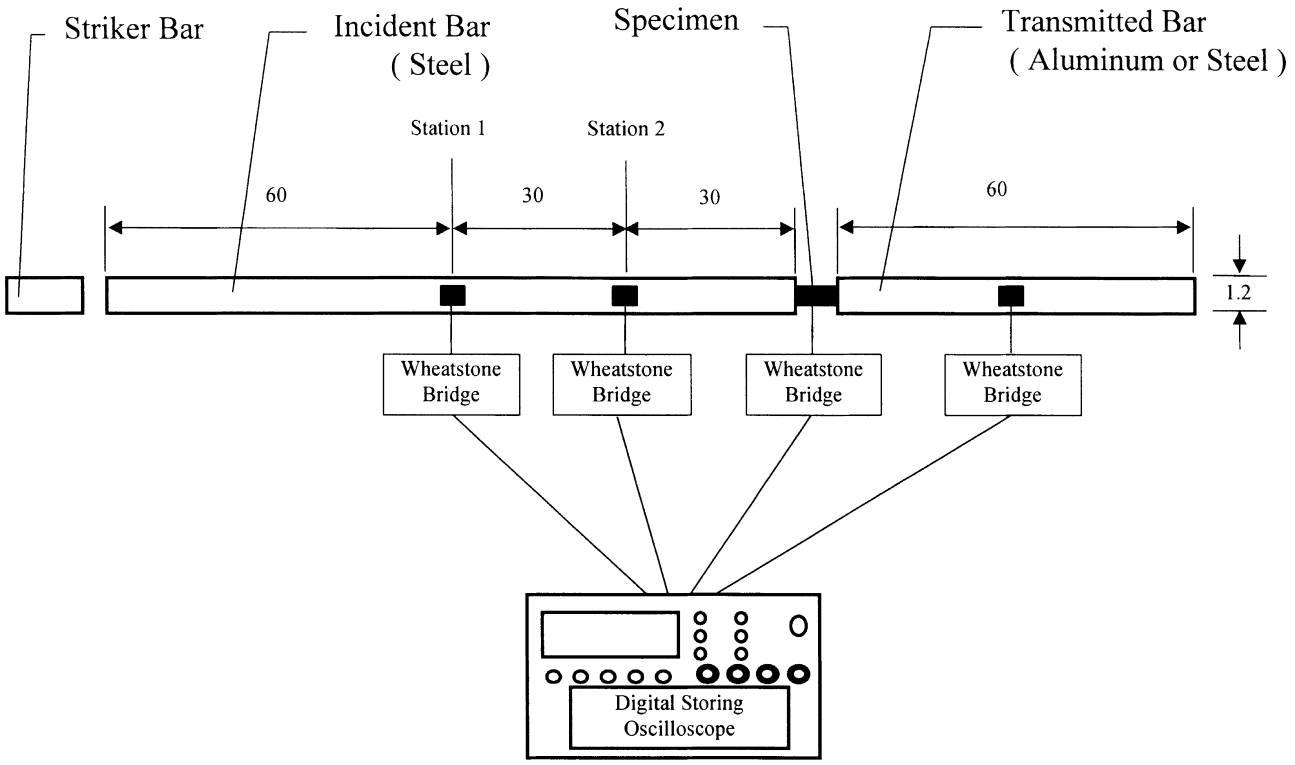

Fig. 1. Schematic illustration of the SHPB setup used. Location of strain gauges is shown. Dimensions are in centimeters.

4. the specimen end surfaces are flat and in perfect contact with the bars for the duration of the experiment.

In the past few decades several investigations have been performed to verify the validity of these assumptions in order to provide higher analysis precision of SHPB experiments. The need to account for wave-dispersion effects in the SHPB was first investigated by Hsieh and Kolsky [6]. A scheme to correct for dispersion based on the first mode of the Pochhammer-Chree dispersion relation was first proposed by Gorham [7] and Follansbee and Frantz [8]. In their work, the correction was successfully applied to SHPB testing of ductile metallic materials. A similar dispersion correction technique was used by Gong et al. [9] when testing the dynamic behavior of concrete. Various modifications were made by other researchers [10–12]. While investigating assumption 2, Chen et al. [13] and Ravichandran and Subhash [14] studied the effect of specimen geometry and presented the concepts of stress homogeneity time and critical strain rate, which is especially important for brittle materials. Bertholf and Karnes [15] found that adequate specimen lubrication eliminated the concerns of radial inertia and friction, thus satisfying assumption 3.

In this work, we revisit some of the critical assumptions of the SHPB operation. Some improvements and modifications as well as a consistent way of performing data analysis are presented. An experimental procedure for determining the stress homogenization time is presented and used as a basis for objective determination of the zero points of the incident, reflected and transmitted waves. The proposed SHPB analysis technique is then used to investigate rate sensitivity over a range of strain rates of a graphite/epoxy composite material.

2. Wave dispersion in a single bar

The dispersion relation for the problem of a longitudinal wave traveling in an infinitely long cylindrical linear elastic bar was first established independently by Pochhammer [16] and Chree [17]. Tabulated results of the Pochhammer-Chree solution can be found in Bancroft [18]. This solution, although not strictly valid for a finite length bar, has in the past been used successfully to correct for wave dispersion effects in the SHPB setup, in cases where bars with large length/diameter ratio were used. This was done for the case of metals in the work of Follansbee and Frantz [8] and for concrete in the work of Gong et al. [9] In this section we will revisit the dispersion correction procedure with emphasis on the details of the method, especially as applied to brittle polymeric matrix composites.

2.1. Methodology for dispersion correction

Assume that the time variation of the stress signal input onto one end of a circular rod can be expressed as

$\sigma = \sigma_0 f(t)$ where σ_0 is the amplitude of a forcing function $f(t)$. The Fourier series expansion of $f(t)$ can be expressed in a discrete form as

$$f(n\Delta t) = \frac{A_0}{2} + \sum_{k=1}^{K}[A_k \cos(k\omega_0 n\Delta t) + B_k \sin(k\omega_0 n\Delta t)], \tag{4}$$

where Δt is the time interval of sampling. And $n = 0, 1, 2, \ldots, N-1$, with N being the number of discretized time points. Also, A_0, A_k and B_k can be calculated by

$$\begin{aligned} A_0 &= \frac{2}{T}\int_0^T f(t)\,\mathrm{d}t, \\ A_k &= \frac{2}{T}\int_0^T f(t)\cos(k\omega_0 t)\,\mathrm{d}t, \\ B_k &= \frac{2}{T}\int_0^T f(t)\sin(k\omega_0 t)\,\mathrm{d}t \end{aligned} \tag{5}$$

and ω_0, the fundamental frequency, is defined as

$$\omega_0 = \frac{2\pi}{T} = \frac{2\pi}{N\Delta t}, \tag{6}$$

where T is the period of $f(t)$. In the event that $f(t)$ is not periodic, as is the case in the SHPB situation, T is replaced by the width of stress pulse time window. Note that a finite number K instead of ∞ symbol is used in the summation of Eq. (4). This truncation represents the fact that in a realistic situation only a finite number of frequencies can be sampled. The particular value of K is related to the bandwidth of the recording device used in the experimentation and thus to the Nyquist frequency. Only frequencies below the Nyquist frequency should be included in the summation of Eq. (4). Inclusion of higher frequencies will introduce aliasing. Thus, the maximum K is limited by the number of sampled time points N, as $K = N/2$ (with $\omega_K = K\omega_0$ corresponding to the Nyquist frequency).

To perform a dispersion correction in the discretized time domain we need to shift the phase of each sine and cosine term in Eq. (4) by an amount related to the propagation velocity of their particular frequency.

We call ϕ_{dk} the phase change after the particular frequency component $k\omega_0$ travels a distance Δx. It can be expressed as

$$\phi_{dk} = k\omega_0 \frac{\Delta x}{c_k}, \tag{7}$$

where c_k is the value of phase velocity corresponding to $k\omega_0$ and is obtained from Pochhammer-Chree solution. Δx is positive for forward dispersion correction and negative for backward correction. Reconstruction of the stress pulse after it has traveled a distance Δx is obtained by summation of all frequencies up to $K\omega_0$,

$$F(n\Delta t) = \frac{A_0}{2} + \sum_{k=1}^{K}\left[A_k \cos\left(k\omega_0 n\Delta t - \frac{\Delta x}{c_k}\right) + B_k \sin\left(k\omega_0 n\Delta t - \frac{\Delta x}{c_k}\right)\right], \tag{8}$$

where $F(n\Delta t)$ is the new form of $f(n\Delta t)$.

The dispersion correction scheme adopted here is slightly different from that of Follansbee and Frantz [8] and of most other previous studies. In the work of Follansbee and Frantz [8], the phase shift used included the term $\Delta x/c_0$ where c_0 is the velocity of propagation of the fundamental frequency ω_0. In Eq. (8), this has been omitted. By omitting this term it is possible to visualize the whole pulse traveling in x as well as t. (See Section 2.3 for more details.)

2.2. Nyquist frequency

The Nyquist frequency of a data acquisition system can be calculated by $f_N = 1/(2\Delta t)$, where Δt is the time interval between two consecutive sampling points. Since this restricts the number of frequencies that can be recorded in an experimental setup, it is intimately related to any attempts at dispersion correction in the SHPB. In most previous works, e.g. Follansbee and Frantz [8] and Gong et al. [9], neither the Nyquist frequency nor the sampling rate are quoted. Thus no objective basis for choosing a particular number of frequencies in the dispersion correction procedure was given in those studies. Including either too few or too many frequency terms may induce errors when reconstructing the signal. To check the minimum number of frequencies necessary to accurately reconstruct a signal, the dispersion method described above was applied to the propagation of an idealized trapezoidal pulse, shown on the left hand side of Fig. 2(a) as the original signal. The trapezoidal pulse illustrated is the same as that used in the work of Follansbee and Frantz [8]. The right hand side of Fig. 2(a) shows the pulse after propagating forward a distance of 0.6 m. The dispersion effect is clearly visible in the distortion of the propagating pulse. It can be seen that the resulting dispersed pulses when using $K = 615$ (i.e. cut-off at the Nyquist frequency) in Eq. (8) and $K = 50$, are similar in rise time and initial peak. However the remainder of the pulse is not well captured when using $K = 50$. (Note that in the work of Gong et al. [9], 55 frequencies were used.) If $K = 25$, the propagated pulse appears highly distorted.

Of more interest when correcting for the strain pulses obtained in a SHPB is the reverse propagation simulation. Fig. 2(b) shows the results of propagating a pulse backward in time (i.e. up the bar). The original pulse (on the right-hand side of Fig. 2(b)) is the forward propagated pulse resulting from the trapezoid of Fig. 2(a) and using $K = 615$ (i.e. cut-off at the Nyquist frequency).

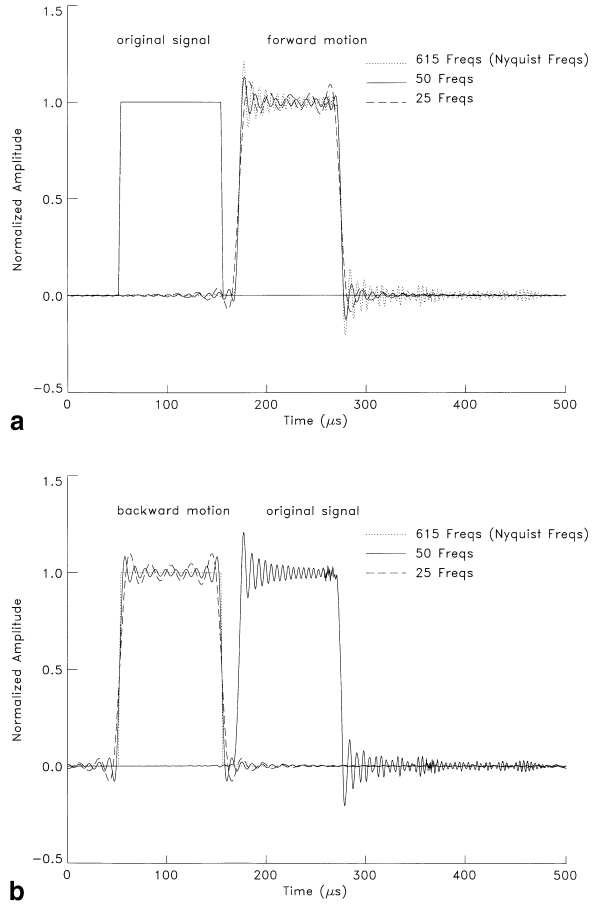

Fig. 2. Effect of number of frequencies on wave dispersion. (a) Forward propagation. (b) Backward propagation.

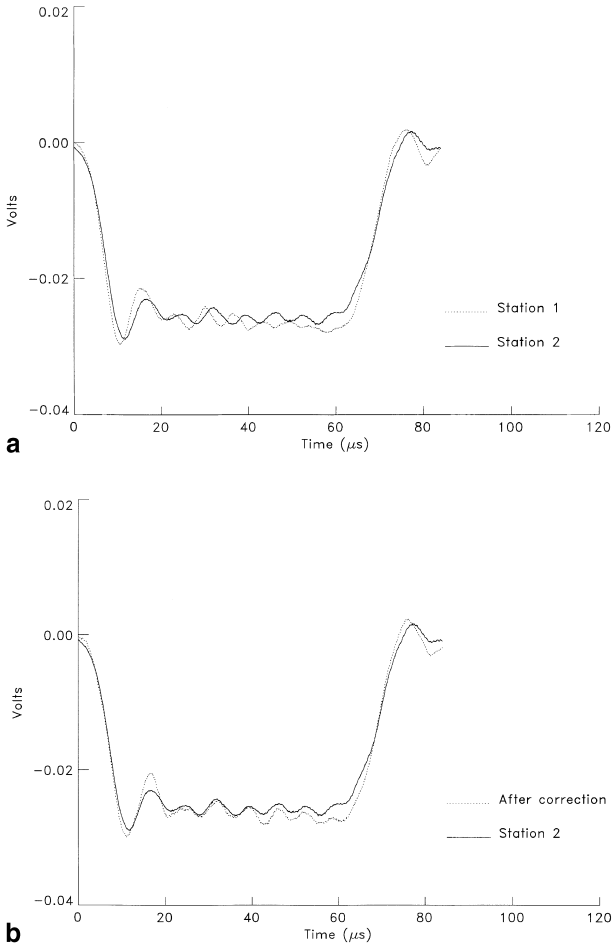

Fig. 3. (a) Original signals from stations 1, 2 in Fig. 1. (b) Dispersion corrected signal from station 1 superposed with original signal from station 2.

This simulates a data acquisition system that has a fixed sampling rate. When this pulse is propagated backwards using $K=615$ the original trapezoid is recovered exactly. Thus using Nyquist frequency as the cut-off in the dispersion correction will ensure exact reproducibility of the actual signal. It can be seen from Fig. 2(b) that when using, for example, $K=50$ or $K=25$, we do not exactly recover the original trapezoid. We have seen that using 80% of the Nyquist frequency as a cut-off (i.e. 500 frequencies in this case) reproduces the original trapezoid with sufficient accuracy (i.e. the error of matching peaks is within 1%). Note, however, that the specific number of frequencies needed to obtain sufficient accuracy may vary depending on the shape of the original signal. For example, for the case of a triangular input pulse, 90% of Nyquist frequency must be used as a cut-off to recover the same accuracy (i.e. within 1% of the original).

Fig. 3(a) shows the pulses recorded at station 1 and 2 of the incident bar (see Fig. 1) in an actual SHPB experiment. Fig. 3(b) shows the as recorded signal at station 2 superimposed with that of station 1 after the latter has been shifted forward using the dispersion correction with the Nyquist frequency as a cut-off. As can be seen the signals are now in phase.

2.3. Dispersion window

In conventional SHPB dispersion analysis, as in, for example, Gong et al. [9] and Lifshitz and Leber [11], the shifting scheme

$$\phi_{dk} = k\omega_0\left(\frac{\Delta x}{c_k} - \frac{\Delta x}{c_0}\right), \tag{9}$$

where variables have been defined before, was used. This is the same as Eq. (7) but with the addition of the term $\Delta x/c_0$. The appearance of the term $\Delta x/c_0$ implies that the wave with fundamental frequency ω_0 (corresponding to c_0) is treated as stationary. By considering the phase differences between other frequencies and the fundamental frequency, the dispersion correction is performed "in-place" without a wave traveling. By using this shifting scheme, the width of incident pulse is naturally selected as the width of the dispersion window. The advantage of selecting window width in

this way is that the window width is short, hence the processing time is reduced. By eliminating the term $\Delta x/c_0$ in Eq. (9) and using Eq. (7) instead, the whole wave is allowed to propagate in the x direction. This can be used to determine the importance of choosing an appropriate dispersion window. Fig. 4 shows the propagation of a pulse consisting of only 2 pure sine waves, $f(t) = \sin(\omega_1 t) + \sin(\omega_2 t)$, where $\omega_1 = 1.06 \times 10^5$ rad/s and $\omega_2 = 50\omega_1$. This figure shows the results of the dispersion procedure applied to this $f(t)$ in which the time window chosen was substantial enough to allow for a significant propagation of the pulse. (In this particular case the pulse window was set at 250 μs.) It can be seen that after traveling a certain distance, the two individual sine waves separate since they propagate at different speeds. If we use the conventional shifting scheme (e.g. Eq. (9)) and select the original pulse duration as the window width (e.g. 60 μs), part of high frequency component (which is traveling slower than the low frequency one) will be truncated. In addition, in the conventional shifting scheme an error is introduced by using the term $\Delta x/c_0$ in Eq. (9) to account for the fundamental frequency since it is difficult to precisely determine the value of c_0 [11]. In the proposed scheme both these errors are eliminated.

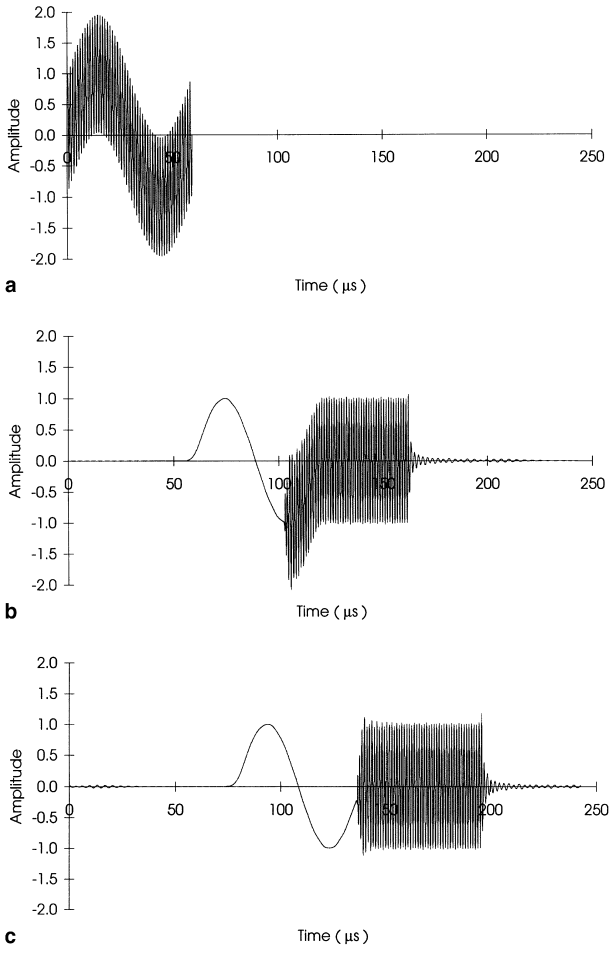

Fig. 4. Dispersion induced pulse separation in a pulse consisting of 2 pure sine waves. (a) Initial pulse. (b) Pulse after propagation of 0.3 m. (c) pulse after propagation of 0.4 m.

3. Application to composites and corresponding data reduction

In this section the above described procedure is used to correct for data obtained in actual SHPB experiments on nominally brittle fiber-reinforced polymeric matrix composites. The SHPB used and the analysis procedure employed are discussed in Sections 3.1 and 3.2. In Section 4 a discussion of the results from a series of experiments on composites is presented.

3.1. Time starting points

Since ε_i, ε_t and ε_r are measured at locations away from the specimen/bar interfaces, they cannot be directly used to calculate the response of the testing material. Each signal must be shifted to correspond to the specimen/bar interface locations, i.e. ε_r and ε_t must be shifted backwards in x, t and ε_i must be shifted forwards, while accounting for dispersion in all cases. In addition, careful selection of the starting points for each pulse must be made. The starting points chosen affect both stress and strain measurements in the specimen. In the case in which the estimated time needed to achieve homogenization [14] is of the order of the specimen failure time, as in the case of composites, appropriate choice of time starting points is critical. Typically, in previous studies [8] selection of starting points of all the pulses is made either by visual inspection or by calculating the travel times based on the distance between the bar strain gage and the specimen/bar interface; both of which are highly subjective. Zhao and Gary [12] suggested a method for determining the starting point of each pulse by matching the shapes of simulated waves of a fictitious specimen with the real pulses. We found this method to be rather complex in its application. Instead, we present an alternative method that can provide a consistent way of selecting starting points.

In a typical experiment we need to determine three starting points, one each for the incident, reflected and transmitted pulses. The starting point of the incident pulse is determined by investigating the slope of successive points in the incident signal. If within a certain window (which included 200 sampling points in this study, but may be varied depending on sampling rate and noise), 90% of the measured slopes are negative (corresponding to a compression pulse) then the starting point of this window is taken as the starting point of incident pulse. The 200-point window is shifted in time till this condition is satisfied.

Once the starting point of the incident pulse is determined, the starting points for the reflected and transmitted pulses can be easily found from it. The dispersion window for each pulse is chosen such that the pulse would have enough time to propagate to or from the bar/specimen interface. The reason for this is to include *all* frequencies making up the initial pulse, even the ones traveling slowest, as was demonstrated in Section 2.3. Then each of the three pulses is dispersion-corrected to a location corresponding to either the incident bar/specimen interface or the specimen/transmitted bar interface as appropriate. With the post-dispersion incident pulse held fixed in time (since its starting time has previously been determined) we select the starting point of reflected pulse by shifting the post-dispersion reflected pulse so that the initial peaks of the two match. By doing this, we actually assume the two pulses have the same post-dispersion rise time. Finally, the transmitted pulse starting location is found by matching the slope of transmitted pulse and the curve generated from the summation of post-dispersion incident pulse and reflected pulse. This is a very important step in the analysis procedure. Not only does it determine the starting point of the transmitted pulse, but also it experimentally investigates the force balance on either of the specimen ends. Thus, it forms the condition for achieving a homogeneous specimen stress state in the specimen. By comparing the summation of post-dispersion incident and reflected pulses with the transmitted pulse we are comparing the force at either end of the specimen. Using this procedure we have a method of experimentally determining when homogenization occurs.

Fig. 5 shows the results of the above described correction procedures, i.e. dispersion correction and selection of starting point for an SHPB experiment on a unidirectional composite material (see Section 4). For the dispersion correction the Nyquist frequency has been used as cut-off. Fig. 5 shows the incident (F_i), inverted reflected ($-F_r$) and transmitted (F_t) pulses after dispersion correction and converted to denote force at the respective bar/specimen interface. The pulse F_t represents the force at the transmitted bar/specimen interface location. The pulse $F_i + F_r$, also shown, represents the force at the incident bar/specimen end. As is clearly seen, the incident and reflected waves show good agreement with respect to the location of their peaks after the correction has been applied. Also the transmitted wave compares well with the difference of incident and inverted reflected waves, thus denoting a substantial time of homogeneous deformation.

When testing brittle materials in the SHPB, several researchers [19], have resorted to using specimen mounted strain gauges for a more accurate determination of strain. In such a case we would also have to find the time starting point of this additional signal. This can be easily done by comparing the strain of the strain gauge on the specimen with that deduced for the incident and reflected SHPB pulses.

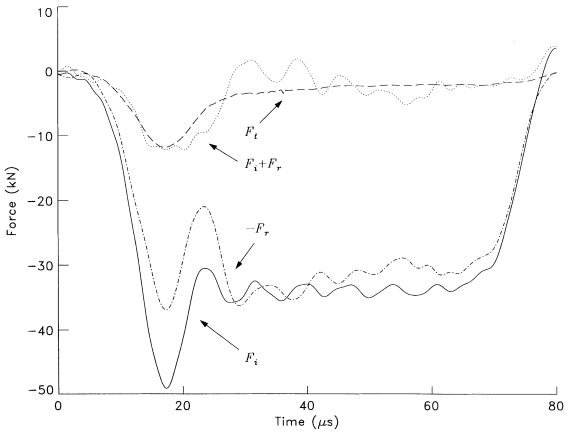

Fig. 5. Force in the bar generated by the incident F_i, inverted reflected $-F_r$, and transmitted pulses F_t. $F_i + F_r$ represents the force on the incident bar/specimen interface; F_t is the force on the specimen/reflected bar interface. Loading is in the fiber direction.

3.2. Stress homogenization and limiting strain rate

One of the basic assumptions of the SHPB is that the stress state in the deforming specimen is homogeneous. Clearly some time is needed for the specimen to achieve a homogeneous stress state after it is first loaded. According to Ravichandran and Subhash [14], this time is approximately $4t_0$, where t_0 is the transit time for the leading edge of the pulse traveling through the specimen. Clearly, it is necessary for the specimen to fail after this time if we are to get a valid failure strength measurement. Any results acquired before the homogenization time should be disregarded. The analysis done by Ravichandran and Subhash is for isotropic, high mechanical impedance, ceramic materials. It needs to be verified before application to anisotropic, lower mechanical impedance, fiber-reinforced composite materials.

When testing composite materials in 1 direction, it is reasonable to expect that 1-D wave propagation theory is still valid since the specimen can be considered as an axisymmetric cylinder. Thus the 1-D result of Ravichandran and Subhash [14] can still be used, except that the ratio of mechanical impedance mismatch, r, between the bar and the specimen must be adjusted accordingly. The mechanical impedance mismatch ratio r is defined as

$$r = \frac{\rho_b c_b A_b}{\rho_s c_s A_s},$$

where ρ, c and A are the density, wave speed and cross section area with the subscripts b and s representing bar

and specimen, respectively. For the material used in this study, this ratio is 16 (as compared to 6–8 for typical ceramic materials). The homogenization ratio $R(t)$ is defined as [14]

$$R(t) = \left| \frac{\sigma_i - \sigma_t}{(\sigma_i + \sigma_t)/2} \right|,$$

where σ_i and σ_t are the axial stresses at the two ends of the specimen. The lower the value of R, the closer the specimen is to a homogeneous stress state. When using a trapezoidal pulse as input, the homogenization curves for different ratios of impedance mismatch are shown in Fig. 6. For comparison purposes, the homogenization ratio computed from a corresponding axisymmetric dynamic finite element analysis using ABAQUS with $r = 16$ is also shown. This plot indicates that impedance mismatch does affect the stress homogenization time; as r increases homogenization occurs sooner. However, there seems to be an underestimation of the homogenization time from the 1-D theory when compared to the corresponding axisymmetric finite element analysis.

The 1-D analysis is certainly not applicable when testing unidirectional composite materials in the 2 and 3 directions because the loading geometry will not possess axisymmetry. Hence 3-D effects need to be included. Since a closed form solution for 3-D wave propagation in anisotropic material is very difficult to obtain, the 3-D dynamic finite element method was chosen to investigate stress homogenization in this case.

The FEM code used was LS-Dyna3D. The problem simulated includes the striker, incident and transmitted bars of the SHPB set up as well as the composite specimen itself loaded in either the 1 or 2 directions. The mesh used is shown in Fig. 7. No-friction contact surfaces are specified at the interfaces between striker/incident bars, specimen/incident bar and specimen/transmitted bar, respectively. The total time duration

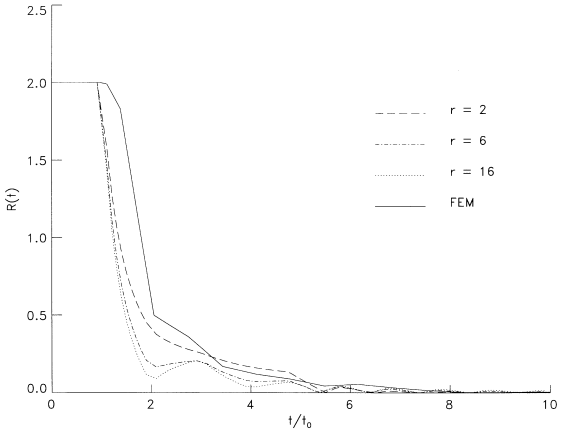

Fig. 6. Stress homogenization in 1 direction by using 1-D wave propagation theory.

analyzed is 160 μs. The specimen is considered as a linear elastic transversely isotropic, strain rate insensitive material with the 2 direction aligned with the bar axis. All the related information about the FEM model, including geometry, material properties, and number of elements etc., are given in Table 1.

The axial stress σ_{zz} in the elements near to the specimen ends is used to calculate the homogenization ratio $R(t)$ defined above. Since we now have a 3-D solution for the elastic stress state, we compute the homogenization ratio at the following locations: the centerline axis of the specimen, the surface of the specimen and the middle line between them. This allows us to investigate homogenization in the radial direction in addition to the axial one. The results of this calculation are shown in Fig. 8. Stress homogenization in the radial and axial directions occurs after about 3 to 4 reflections, as in the case of loading in the 1 direction. Hence the same criterion for determining homogenization time can be used for composite materials in all three directions.

According to the work of Ravichandran and Subhash [14], the limiting strain rate conditions need to be verified for the attainment of valid ultimate failure properties. For brittle materials that show only linear elastic behavior before failure, the nominal strain rate can be approximated by

$$\dot{\varepsilon} = \frac{\varepsilon_f}{t_f},$$

where ε_f and t_f are failure strain and failure time, respectively. Applying the condition $t_f \geqslant 4t_o$, the limiting strain rate can be determined by

$$\dot{\varepsilon} = \frac{\varepsilon_f c_s}{4L_s}.$$

Where $c_s = \sqrt{E_s/\rho_s}$ is the wave speed in the specimen. The significance of this was discussed by Ravichandran and Subhash [14]. Note that this value should be compared to the *average* strain rate in each SHPB experiment in order to assure that it has not been exceeded. Since Young's modulus increases as strain rate increases, using the static value of Young's modulus to calculate c_s and do the above FEM analysis can be considered conservative.

4. Experimental results

It is well-known that many fiber-reinforced polymeric matrix composites are highly rate sensitive [20,21]. However, a satisfactory analytical model that describes their behavior fully does not exist at present, partially because of the lack of reliable macroscopic and microscopic data for these materials. In this part of the study experimentation was carried out to determine the quasi-static and dynamic response of a fiber-reinforced

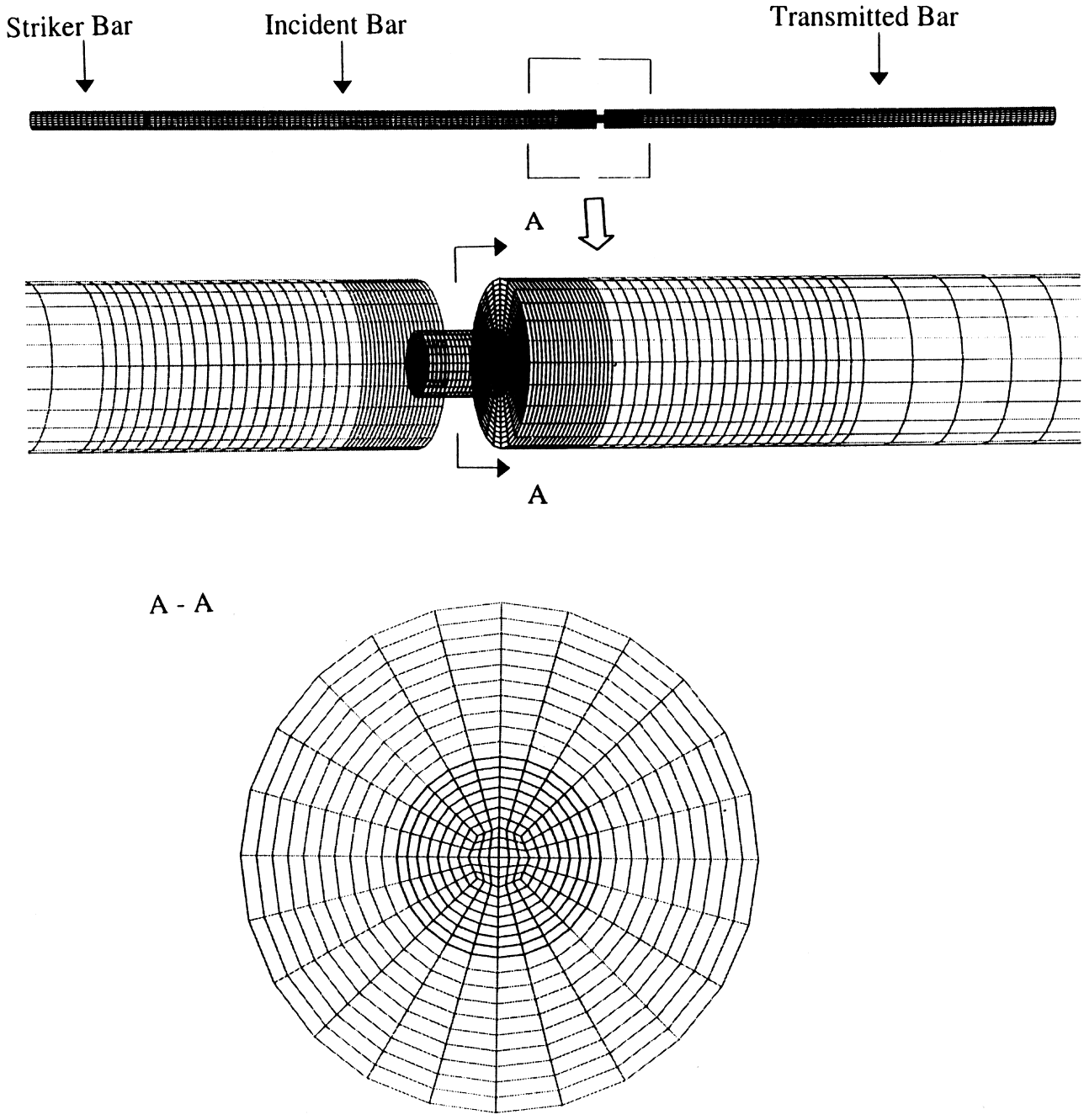

Fig. 7. 3-D FEM model for SHPB.

polymeric matrix composite. The material used was provided by Composite Mirror Applications, Inc. (Tucson, AZ.) from prepreg of AKZO FORTAFIL 3(C)/8804. It is a 48-layer graphite/epoxy unidirectional laminate with fiber volume fraction of 60%. This material is the same as that used in the fracture studies of Lambros and Rosakis [22], and Prabhu and Lambros [23]. The same cylindrical geometry was used for both static and dynamic tests. The nominal diameter of the specimen was 5 mm and the length was 6.5 mm; an aspect ratio of about 1.3, well within the limits set by radial inertia considerations and frictional restraint [15]. We define the fiber direction as 1 and the through-thickness direction as 3. Quasi-static strain rates are produced by means of a hydraulic Instron machine. Dynamic experimentation utilizes the SHPB setup. In the latter case data are analyzed using the procedure described in Section 3. In all cases the sampling rate used was 25 MHz and the Nyquist frequency was used as a cut-off in the dispersion correction.

Typical stress–strain curves from quasi-static compression tests ($\dot{\varepsilon} = 0.0001/s$) in the 1, 2 and 3 directions

Table 1
Parameters for 3-D FEM model

	Striker bar	Incident bar	Transmitted bar	Specimen
Geometry, Length (mm) × Diameter (mm)	80 × 12.7	320 × 12.7	320 × 12.7	6.5 × 5
Type and number of elements	8-node hexahedron solid element	8-node hexahedron solid element	8-node hexahedron solid element	8-node hexahedron solid element
Number of elements per layer × Number of layers	444 × 20	444 × 114	444 × 114	204 × 20
Material properties	E = 205 GPa ρ = 7833 kg/m^3 υ = 0.3	Same as left	Same as left	E_{11} = 142 GPa; $E_{22} = E_{33}$ = 10.3 GPa; $\nu_{21} = \nu_{31}$ = 1.96e-2; ν_{32} = 0.27 $G_{12} = G_{23} = G_{31}$ = 7.2 GPa
Constraints and initial conditions	No constraints. Initial velocity: 25 m/s	No constraints and initial conditions	Same as left	Same as left

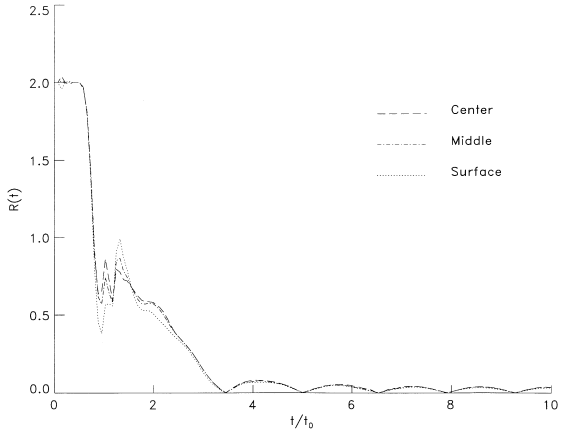

Fig. 8. Stress homogenization in 2 direction at different locations.

are shown in Fig. 9(a)–(c). All quasi-static tests show brittle behavior with the stress–strain curves linear up to failure. In the 1 direction, specimens were observed to fail by axial splitting, sometimes at many locations almost simultaneously. In the 2 and 3 directions, specimens were split into two parts along a direction which was about 45° from the specimen axis. Under quasi-static loading the Young's moduli in the 2 and 3 directions are fairly close; 4.6 GPa and 3.7 GPa respectively. However the failure stress in the 3 direction was seen to be higher than that in the 2 direction. When compression loading is applied in the 3 direction delaminations (debonding between layers) are suppressed, thus increasing ultimate stress values.

In the dynamic tests, specimens in each of the 1, 2 and 3 directions invariably failed in almost the same way as their counterparts in static tests. However their response was substantially rate sensitive. Compression stress–strain curves obtained under dynamic loading are also shown in Fig. 9(a)–(c). In Fig. 9(a) the static as well as two additional stress–strain curves at higher rates are shown. Rate sensitivity as well as damage induced non-linearity regimes are clearly seen. In the dynamic experiments in the 1 direction, stress homogenization occurs at relatively short times. Thus, we can obtain reliable values of Young's modulus from the curves in Fig. 9(a). Clearly Young's modulus can increase substantially (from 69 GPa to 400 GPa) with increasing rate. Note however that the value of Young's modulus is sensitive to dispersion. It may differ by as much as 50% (usually underestimated) before dispersion correction is applied. Thus, when testing brittle solids dispersion correction is absolutely necessary. Fig. 9(b)–(c) shows static and dynamic stress–strain curves for the 2 and 3 directions. The dynamic stress–strain curves for both directions show common characteristics. That is, after the first linear portion, the curve turns into a relatively flat plateau, then climbs up till failure. It must be pointed out, however, that the time for stress

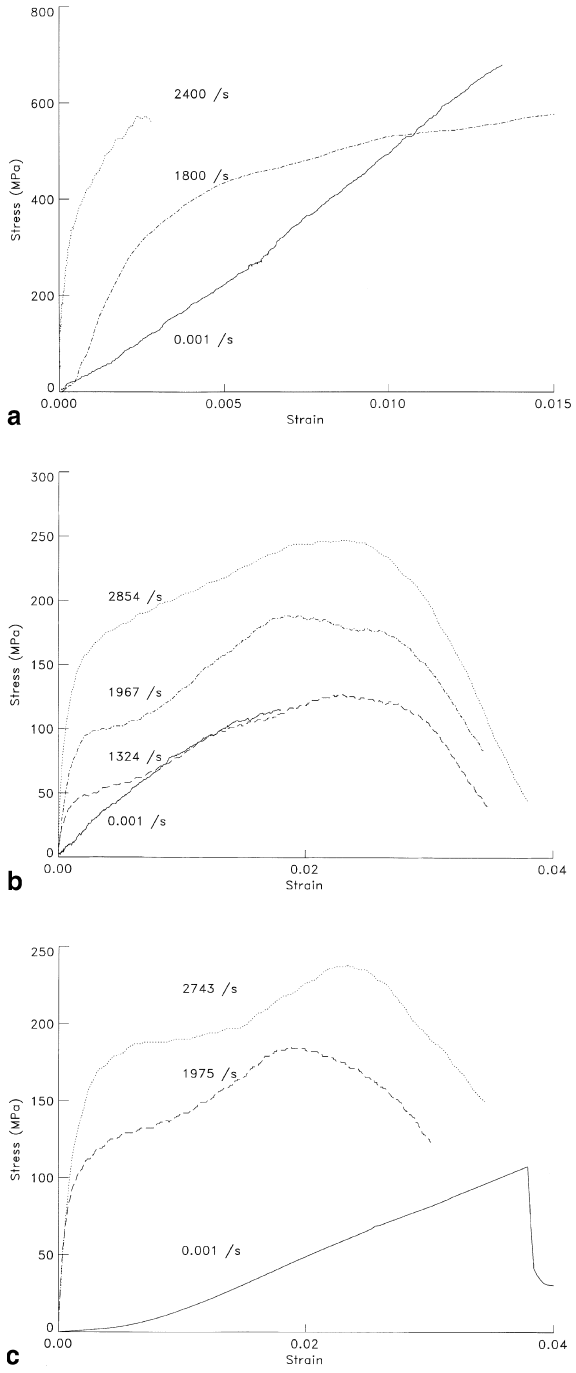

Fig. 9. Stress–strain curves of a range of strain rates for a graphite/epoxy unidirectional composite (a) loading along fibers, i.e. 1 direction; (b) loading in 2 direction; (c) loading through thickness, i.e. 3 direction.

homogenization in this case is substantially larger than that for the 1 direction although it takes the same number of wave reflections within the specimen to get this homogenization. This time usually makes the first linear portion of the stress–strain curve invalid. Thus for the 2 and 3 directions only failure properties can be considered valid, even though the stress–strain curve upon first inspection appears "normal".

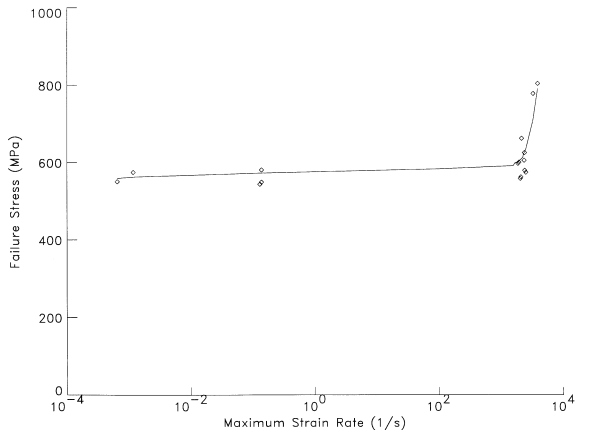

Fig. 10. Failure stress vs. strain rate for loading in the 1 direction.

Fig. 10 shows the dependence of failure stress on strain rate for loading in the 1 direction. Failure stress is roughly constant for a substantial range of strain rates. In the study of Daniel et al. [20] it was concluded that no strain rate sensitivity was present in their particular graphite/epoxy material. However, strain rates only up to 500/s were used. As is seen in Fig. 10, at about 2000/s there is a sharp increase in failure stress. A similar effect was seen in Lankford [21]. Micro-mechanical characterization of the material in each regime is currently underway and the results will be presented in a future study.

5. Conclusions

A SHPB data reduction procedure was presented in this paper. A consistent way of performing data analysis including correction of dispersion, selection of starting points and dispersion window, consideration of stress uniformity and strain rate was presented. The Nyquist frequency is used in the data analysis as the cut-off frequency for dispersion correction. A consistent scheme of determining the starting points in each pulse is proposed based on dispersion and stress homogenization in the specimen. The pulses are shifted accordingly so that close agreement is obtained between the forces on the incident and transmitted end of the specimens for times exceeding the homogenization time.

Experimental results for a graphite/epoxy composite material were also presented. Strain rate sensitivity was observed for loading in all material directions in both elastic and damage regimes. Comparison of the results with and without dispersion correction shows that dispersion correction is necessary for SHPB technique in predicting Young's modulus for composite materials. It is also found that extending the time to failure, e.g. by using the pulse shaping technique [19], might be needed when testing in the 2 and 3 directions since in

the present setup homogenization times are similar to times for failure.

Acknowledgements

We wish to acknowledge the support of ONR Grant No. N00014-93-1-1014 under the supervision of Dr. Y.D.S. Rajapakse and of NSF Grant No. CMS-9622241. We are also grateful for the help from the Center for Composite Materials at University of Delaware. The assistance of Dr. J.R. Vinson and discussions with Mr. Eric Preissner are also appreciated.

References

[1] Kolsky H. An investigation of the mechanical properties of materials at very high rates of loading. Proc Phys Soc 1949;B62:676–700.
[2] Hopkinson B. A method of measuring the pressure in the deformation of high explosives or by the impact of bullets. Phil Trans R Soc 1914;A213:437–52.
[3] Harding J, Wood ED, Campbell JD. Tensile testing of materials at impact rate of strain. J Mech Engrg Sci 1960;2:88–96.
[4] Duffy J, Campbell JD, Hawley RH. On the use of a torsional split Hopkinson bar to study rate effects in 1100-0 aluminum. J Appl Mech 1971;38:83–91.
[5] Nemat-Nasser S, Isaacs JB, Starrett JE. Hopkinson techniques of dynamic recovery experiments. Proc R Soc Lond 1991;A435:371–91.
[6] Hsieh DY, Kolsky H. An experimental study of pulse propagation in elastic cylinders. Proc Phys Soc 1958;71:608–12.
[7] Gorham DA. A numerical method for the correction of dispersion in pressure bar signals. J Phys E Sci Instr 1983;16:477–9.
[8] Follansbee PS, Frantz C. Wave propagation in the split Hopkinson pressure bar. J Engrg Mat Tech 1983;105:61–6.
[9] Gong JC, Malvern LE, Jenkins DA. Dispersion investigation in the split Hopkinson pressure bar. J Engrg Mat Tech 1990;112:309–14.
[10] Lee CKB, Crawford RC. A new method for analysis dispersed bar gauge data. Mater Sci Technol 1993;4:931–7.
[11] Lifshitz JM, Leber H. Data processing in the split Hopkinson pressure bar tests. Int J Impact Engrg 1994;15:723–33.
[12] Zhao H, Gary G. On the use of SHPB techniques to determine the dynamic behavior of materials in the range of small strains. Int J Solids Structures 1996;33:3363–75.
[13] Chen W, Subhash G, Ravichandran G. Evaluation of ceramic specimen geometries used in split Hopkinson pressure bar. DYMAT J 1994;1:193–210.
[14] Ravichandran G, Subhash G. Critical appraisal of limiting strain rates for compression testing ceramics in a split Hopkinson pressure. J Am Ceram Soc 1994;77:263–7.
[15] Bertholf LD, Karnes CH. Two-dimensional analysis of the split Hopkinson pressure bar system. J Mech Phys Solids 1975;23:1–19.
[16] Pochhammer L. Uber die fortpflanzungsgeshwindigkeiten kleiner schwingungen in einem unbergrenzten isotropen kreiszylinder. J Reine Angewandte Mathematik 1876;81:324–36.
[17] Chree C. The equations of an isotropic elastic solid in polar and cylindrical co-ords., their solutions and applications. Cambridge Phil Soc Trans 1889;14:250–369.
[18] Bancroft D. The velocity of longitudinal waves in cylindrical bars. Physical Review 1941;59:588–92.
[19] Chen W. Dynamic failure behavior of ceramics under multiaxial compression, Ph.D. thesis, California Institute of Technology, 1995.
[20] Daniel IM, Hamilton WG, LaBedz RH. Strain rate characterization of unidirectional graphite/epoxy composite. Composite Materials: Testing and Design (Sixth Conference), ASTM STP 787;1982:393–413.
[21] Lankford J. Compressive damage and failure at high loading rates in graphite fiber-reinforced polymeric matrix composites. Ceramic Transaction 1991;19:553–63.
[22] Lambros J, Rosakis AJ. Dynamic crack initiation and growth in thick unidirectional graphite/epoxy plates. Composites Science and Technology 1997;57(1):55–65.
[23] Prabhu S, Lambros J. Three dimensionality and K-dominance effects in the fracture of anisotropic solid. J Compos Mater, submitted for publication.